EUROPEAN ORGANIZATION FOR NUCLEAR RESEARCH
ORGANISATION EUROPEENNE POUR LA RECHERCHE NUCLEAIRE

CERN – AB DIVISION

AB-Note-2004-021 BDI

IMPROVING FFT FREQUENCY MEASUREMENT RESOLUTION BY PARABOLIC AND GAUSSIAN INTERPOLATION

M. Gasior, J.L. Gonzalez

Abstract

Discrete spectra can be used to measure frequencies of sinusoidal signal components. Such a measurement consists in digitizing a compound signal, performing windowing of the signal samples and computing their discrete magnitude spectrum, usually by means of the Fast Fourier Transform algorithm. Frequencies of individual components can be evaluated from their locations in the discrete spectrum with a resolution depending on the number of samples. However, the frequency of a sinusoidal component can be determined with improved resolution by fitting an interpolating parabola through the three largest consecutive spectrum bins corresponding to the component. The abscissa of its maximum constitutes a better frequency approximation. This method has been used for tune measurement systems in circular accelerators. After a review of the method, the paper describes the efficiency of the interpolation, depending on the windowing formula applied to signal samples. Some windows allow the parabolic interpolation to increase the frequency measurement resolution by more than one order of magnitude. The aim of this paper is also to show that even better results are obtained using Gaussian interpolation. Such a method yields an improvement of more than two orders of magnitude with windows having very good spectral properties. An improvement beyond three orders of magnitude is possible with Gaussian windows. These results are confirmed by measurements.

Geneva, Switzerland
February 2004

1. Introduction

Discrete spectra can be used to measure frequencies of sinusoidal signal components. Such a measurement consists in digitizing a compound signal, performing windowing of the signal samples and computing their discrete magnitude spectrum, usually by means of the Fast Fourier Transform (FFT) algorithm. Frequencies of individual components can be evaluated from their locations in the discrete spectrum with a resolution depending on the number of samples. However, the frequency of a sinusoidal component can be determined with improved resolution by fitting an interpolating parabola through the three largest consecutive spectrum bins corresponding to the component. The abscissa of its maximum constitutes a better frequency approximation. This method has been used for tune measurement systems in circular accelerators **[1]**. After a review of the method, the paper describes the efficiency of the interpolation, depending on the windowing formula applied to signal samples. Some windows allow the parabolic interpolation to increase the frequency measurement resolution by more than one order of magnitude. The aim of this paper is also to show that even better results are obtained using Gaussian interpolation. Such a method yields an improvement of more than two orders of magnitude with windows having very good spectral properties. An improvement beyond three orders of magnitude is possible with Gaussian windows. These results are confirmed by measurements.

2. FFT frequency measurement

The following example illustrates some of the practical issues of signal frequency measurements. **Figure 1** shows the magnitude spectrum of a signal containing many frequency components. Suppose the frequency of the component of interest lies within the range f_{min} to f_{max}, and the peak corresponding to this component constitutes a local maximum only in that range. Because there are some other large peaks outside the range, it is, however, not possible to measure this frequency directly, e.g. using an ordinary frequency meter based on counting input signal periods within a reference time.

One way to measure this frequency could be to use a band-pass filter with cut-off frequencies f_{min} and f_{max}. Nevertheless, building such a filter is particularly difficult when the pass band is wide and strong undesirable components are located nearby. A common alternative approach is, therefore, to perform a Fourier analysis of the sampled signal and then search for the local maximum within the range of interest.

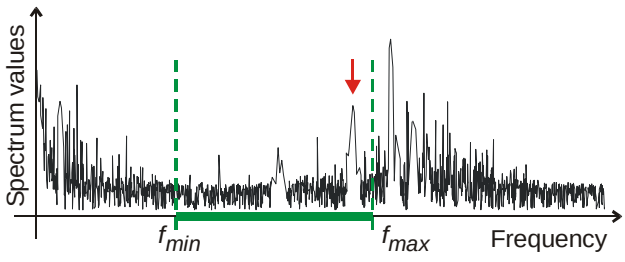

Fig. 1. Example of a magnitude spectrum. The frequency of interest lies within the range f_{min} to f_{max} and the peak pointed by the arrow, corresponding to this frequency, constitutes the local maximum only in that range. Outside the range there are much stronger components.

Assume that a bandlimited compound signal

$$s(t) = \sum_l A_l \sin(2\pi f_l t) + A_{in} \sin(2\pi f_{in} t) \tag{1}$$

has been uniformly sampled with frequency f_s and contains a sinusoidal component $s_{in}(t)$, whose frequency f_{in} is to be measured. The Discrete Fourier Transform (DFT) magnitude spectrum $S[k]$ of the sampled signal, usually computed using the FFT [(1)] algorithm, is given by

$$S[k] = \left| \sum_{n=0}^{N-1} s[n] \exp\left(-\mathrm{j} \frac{2\pi n k}{N} \right) \right| \tag{2}$$

where $s[n]=s(nT_s)$ is the signal sample sequence, $T_s=f_s^{-1}$ is the sampling period and N is the total number of samples.

The discrete spectrum (2) is calculated at frequencies that are integer multiples of Δ_f, and

$$\Delta_f = \frac{f_s}{N} \tag{3}$$

If discrete magnitude spectrum $S[k]$ has a local maximum corresponding to component $s_{in}(t)$ at spectrum bin k_m, its frequency f_{in} can be approximated as

$$f_{in} \cong f_m = k_m \Delta_f = k_m \frac{f_s}{N} = \frac{k_m}{N T_s} = \frac{k_m}{L} \tag{4}$$

where $L=N T_s$ is the sampling duration of the input signal.

When frequency f_{in} is estimated using (4), the largest error occurs for a frequency located in the middle between two discrete spectrum bins. This error may be interpreted as the resolution of an FFT frequency measurement method. Denoting the largest frequency error as ε one gets

$$\varepsilon = \max \left| k_m \Delta_f - f_{in} \right| = \frac{1}{2} \Delta_f = \frac{f_s}{2N} = \frac{1}{2NT_s} = \frac{1}{2L} \tag{5}$$

When the frequency error is expressed in units of Δ_f (see (5)), it is independent of N. For that reason Δ_f is often used in the paper as a convenient unit of frequency measurement errors.

Note that the biggest relative frequency error

$$\varepsilon_r = \frac{\varepsilon}{f_{in}} = \frac{1}{2N} \frac{f_s}{f_{in}} \cong \frac{1}{2k_m} \tag{6}$$

increases for decreasing input frequencies and constant sampling rate. For this reason, the relative error of a FFT frequency measurement becomes very large for components lying on the discrete spectrum beginning.

[(1)] Term FFT is also used in the paper as a practical equivalent of DFT.

3. Discrete spectrum interpolation

Equation (5) suggests two potential ways of improving the FFT frequency measurement resolution:

- Increase the size of the FFT input data set.
  Since the calculation time of an N-point FFT is proportional to $N \log_2(N)$, a resolution expansion of one order of magnitude will increase the calculation time by more than one order of magnitude. Bigger N means also longer acquisition time L.
- Decrease the sampling frequency.
  The sampling theorem determines the smallest sampling frequency. Usually its practical value is higher than the theoretical limit, due to the finite slope of the frequency characteristics of a low-pass antialias filter. Furthermore, for some applications may be favorable to use still higher sampling frequency (oversampling) at the expense of deteriorating the spectrum resolution. Therefore, this approach offers little opportunity for frequency measurement resolution improvements.

When abovementioned means have been employed to the limits and still the frequency resolution offered is not sufficient, or, if it is needed to reduce the frequency measurement time and conserve the resolution, a discrete spectrum interpolation can be used. This approach has already been used in betatron tune measurement systems **[1, 2, 3, 4, 5, 6]**. The method principle is sketched in **Fig. 2**.

When the measured frequency component f_{in} is located exactly on a local maximum peak of the discrete spectrum at bin k_m, frequency f_{in} can be calculated according to (4) with no error. This is the ideal case shown in **Fig. 2a**. When f_{in} increases, the amplitude of spectrum bin k_m–1 gets smaller and of bin k_m+1 bigger, as presented in **Fig. 2b**. The spectrum value $S[k_m]$ remains the biggest, until f_{in} is equidistant between bins k_m and k_m+1, see **Fig. 2c**. In this case, determining f_{in} with (4) leads to the biggest error (5). When f_{in} is increased further, as shown in **Fig. 2d**, bin k_m+1 becomes the biggest. For f_{in} smaller than $k_m\Delta_f$, the analysis is similar resulting in symmetrical cases.

This example illustrates the fact that frequency f_{in} of the continuous spectrum can be estimated, even if it is located between two discrete spectrum bins, by calculating the maximum abscissa of an interpolation curve of the discrete spectrum peak. This maximum can be located between k_m–$^1/_2$ and k_m+$^1/_2$, where k_m is the index of the biggest bin within the range of interest. If one needs to resolve the cases presented in **Fig. 2** and symmetrical ones, it is necessary for the interpolation to have at least three node points. Such three-node interpolation methods, when used in conjunction with an appropriate window, can give improvements of frequency measurement resolution beyond three orders of magnitude.

If in the (continuous-time) Fourier Transform (FT)

$$S(f) = \int_{-\infty}^{\infty} s(t) \exp(-\mathrm{j}2\pi f t) dt \tag{7}$$

one assumes time domain sampling $t = nT_s$ and frequency domain sampling $f = k\Delta_f$, then the integral can be replaced by a sum with N elements and FT (7) becomes DFT as in (2) when taking T_s and Δ_f as units in the discrete time and frequency domains. For this reason discrete spectra in the paper are considered as continuous spectrum samples taken at multiplies of Δ_f, allowing to examine discrete spectra between bins by means of the FT (7).

Replacing the ordinary frequency f in (7) by

$$\varphi = \frac{f}{\Delta_f} = \frac{N}{f_s} f = NT_s f = Lf \tag{8}$$

referred to as the normalized frequency, adjusts continuous spectra to the scale of the discrete spectrum bin indexes. It allows expressing discrete and continuous spectra in one convenient scale (e.g. φ=100.5 for frequency lying exactly between bin 100 and 101).

3.1. Parabolic interpolation

Let $S[k]$ be the discrete magnitude spectrum of a signal containing a sinusoidal component of frequency f_{in}, and k_m be the index of the biggest bin of the corresponding discrete spectrum peak. Index k_m can be found if the bin constitutes a local maximum within a given range. Fitting a parabola

$$S_p(\varphi) = a(\varphi - \varphi_m)^2 + h \tag{9}$$

through interpolation nodes $S[k_m-1]$, $S[k_m]$ and $S[k_m+1]$, and finding the abscissa of the interpolation maximum, gives

$$\varphi_{in} \cong \varphi_m = k_m + \Delta_m = k_m + \frac{S[k_m+1] - S[k_m-1]}{2\left(2S[k_m] - S[k_m+1] - S[k_m-1]\right)} \tag{10}$$

provided that coefficient a in (9) is negative, which implies $2S[k_m] > S[k_m+1] + S[k_m-1]$.

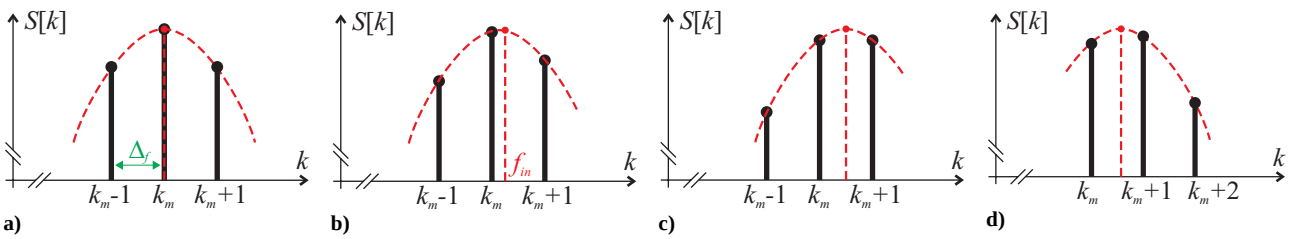

Fig. 2. Principle of three-node interpolation methods. In Fig. a) the continuous spectrum maximum lies exactly on the biggest bin of the discrete spectrum peak. In Fig. b) the frequency of the maximum is larger than that of the biggest bin. Figure c) shows the case where the maximum is exactly between two equal bins. In Fig. d) next bin becomes the largest and the frequency of the continuous spectrum maximum is already smaller than that corresponding to this bin.

The quantity Δ_m in (10) is the abscissa correction of the discrete spectrum maximum. It is a real number ranging from $-1/2$ when $S[k_m-1]=S[k_m]$, to $1/2$ when $S[k_m+1]=S[k_m]$. It links the index k_m of the biggest bin of the discrete spectrum peak and the maximum abscissa φ_m of the interpolating curve peak. Normalized frequency φ_m designates the abscissa approximation of the local maximum of the continuous spectrum $S(\varphi)$ at frequency φ_{in}.

The abscissa approximation φ_m of the continuous spectrum maximum can be, at the most, at a distance $1/2$ from the largest bin of the discrete spectrum peak and for efficient interpolation one node point on each side of the peak maximum is necessary. In consequence, the minimal width of the continuous spectrum peak is three bins. This is also necessary for other three-node interpolation methods. To satisfy this condition, a special function, called a window, has to be applied to the signal samples. This multiplicative process named windowing, which can be considered also as a modulation, gives to the spectral peak the shape of the Fourier transform of the window function. If no special windowing is performed, the sampling beginning and end set implicitly a rectangular window.

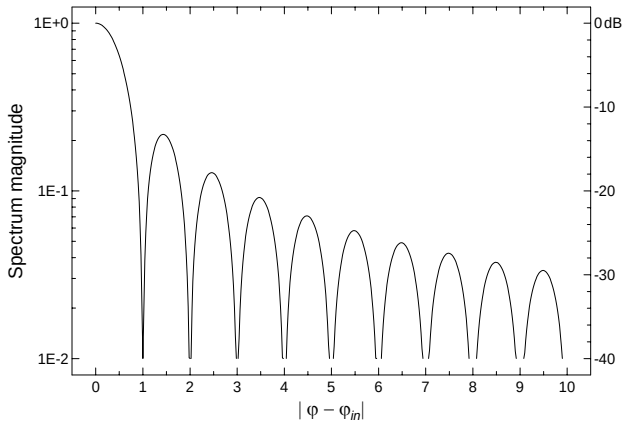

Fig. 3. Magnitude spectrum around the maximum at φ_{in}, when using rectangular windowing. The right vertical axis is scaled in dB referred to 1.000, the main lobe maximum. The highest sidelobe is only –13.3 dB below main lobe.

Let $w_r(t)$ be a rectangular window of length L, which is symmetrical with respect to $t=0$. It has the form of

$$w_r(t)=\frac{1}{L}\left(H\left(t+\frac{L}{2}\right)-H\left(t-\frac{L}{2}\right)\right) \qquad (11)$$

where $H(t)$ is the Heaviside unit step function.

If this window is applied to a signal containing a sinusoidal component of frequency f_{in}, the resultant magnitude spectrum has a peak with maximum at f_{in} and a shape given by the windowing function Fourier transform

$$W_r(f_o)=\left|\frac{\sin(\pi L f_o)}{\pi L f_o}\right| \qquad (12)$$

where $f_o=f-f_{in}$ is the offset from the input frequency.

Spectrum (12) has been calculated using the continuous Fourier transform. It can be scaled to the "discrete spectrum" units by replacing the ordinary frequency f by the normalized frequency $\varphi = N T_s f = L f$ (8)

$$W_r(\varphi_o)=\left|\frac{\sin(\pi\varphi_o)}{\pi\varphi_o}\right| \qquad (13)$$

where $\varphi_o=\varphi-\varphi_{in}$ is the frequency offset from φ_{in}.

The magnitude spectrum is shown in **Fig. 3**.

The main lobe of the rectangular windowing spectrum (13) extends on 2 bins, so it is too narrow for efficient spectrum interpolation. In the Appendix there are given further details.

Better windows can improve both, the interpolation efficiency and the amplitude dynamics of the FFT frequency measurement, by reducing spectral leakage, which is very large with rectangular windowing (i.e.

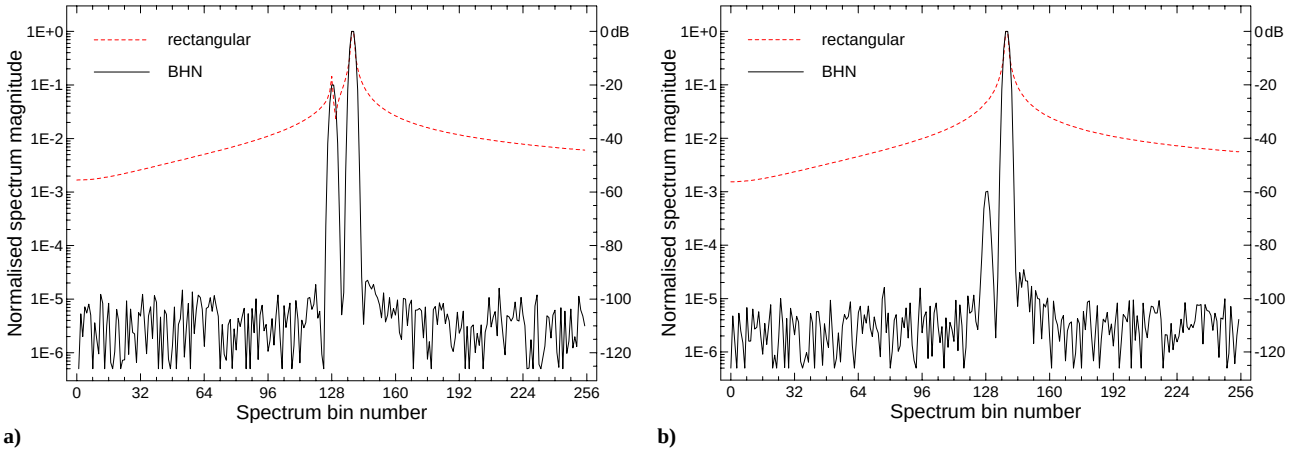

Fig. 4. Both figures show part of 2048-point spectra of a simulated signal, scaled and rounded to 14-bit full-scale samples. The signal contains two sinusoidal components with very disparate amplitudes, but with similar frequencies, located at φ=128.5 and φ=138.5 (i.e. exactly between spectrum bins to maximise the leakage effect). In Fig. a) the amplitude ratio of the signal components is 10 (20dB) and in Fig. b) 1000 (60dB). When the rectangular window is used (dashed lines), the spectrum is distorted by the leakage and small components are drowned, as in Fig. b). Even small components can be distinguished when the signal is properly windowed to minimise the leakage (solid lines – Blackman-Harris-Nuttall window).

without using any explicit window). The spectral leakage effect is a consequence of the fact that the transform in (2) assumes that the input data are samples of a periodic signal of period $L = N T_s$. The purpose of windowing is therefore to attenuate the signal samples close to the boundaries, so that the adjacent periods of the hypothetical signal fit smoothly. In the frequency domain this is equivalent to preventing the energy of adjacent bins from spreading, as it happens with the rectangular window spectrum shown in **Fig. 3**.

Properties of different windows have been widely discussed **[7, 8]** and this paper does not deal with them in detail. The only concern for three-node interpolation methods is that the spectrum main lobe corresponding to the component of interest must extend at least on three bins. As an example, a modified Blackman-Harris window, later called the Blackman-Harris-Nuttall (BHN) window **[8]**, satisfies this condition and reduces the leakage to improve resolvability of small signal components. **Figures 4a** and **4b** show a comparison between BHN and rectangular windowing.

The BHN window is defined as

$$w_{bhn}(t) = w_r(t) \sum_{i=0}^{3} c_i \cos\left(\frac{2\pi i}{L} t\right) \qquad (14)$$

where $c_0 = 0.355768$, $c_1 = 0.487396$, $c_2 = 0.144232$, $c_3 = 0.012604$ and $w_r(t)$ is the rectangular window (11).

The window shape is shown in the Appendix in **Fig. A-1**.

When a signal containing a component of frequency f_{in} is windowed with the BHN window (14) of length L, its magnitude spectrum has a local maximum at $\varphi_{in} = f_{in} L$, and the spectrum is given by

$$W_{bhn}(\varphi_o) = \left| \frac{\varphi_o}{\pi} \sin(\pi \varphi_o) \sum_{i=0}^{3} \frac{(-1)^i c_i}{\varphi_o^{\,2} - i^2} \right| \qquad (15)$$

for $\varphi_o = \varphi - \varphi_{in}$.

The magnitude spectrum is shown in **Fig. 5**. The main lobe extending on eight bins is suitable for the parabolic interpolation method.

An example of the parabolic interpolation on the main lobe of the BHN windowing spectrum (15) is presented in **Fig. 6**. The solid curve corresponds to the normalized continuous spectrum (15) of a sinusoidal signal with normalized frequency $\varphi_{in} = 128.25$. The three marks on the curve are the amplitudes of the discrete spectrum bins used as three nodes of the parabolic interpolation centered in k_m. The dashed line shows the parabola fit through these nodes. The abscissa φ_m of the maximum is calculated from equation (10) and $\varphi_d = \varphi_{in} - k_m$ is the displacement of the input frequency φ_{in} from the fitting center k_m (index of the biggest bin within the range of interest).

In the ideal case, the normalized frequency φ_m obtained by interpolation, should be equal to φ_{in}, the actual frequency of the signal component of interest. The interpolation error $E(\varphi_d)$ observed in the measurements is therefore

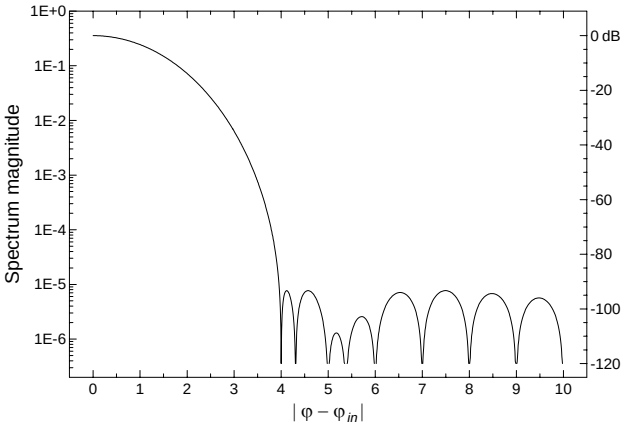

Fig. 5. The magnitude spectrum around the local maximum at φ_{in}, when using Blackman-Harris-Nuttall windowing. The right vertical axis is scaled in dB, referred to 0.356, the main lobe maximum.

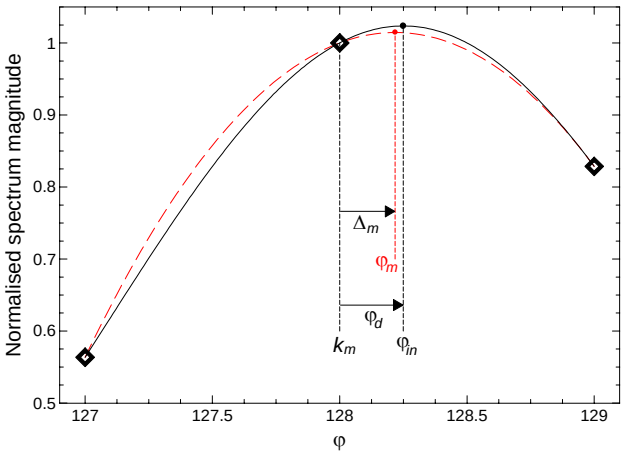

Fig. 6. Example of the parabolic interpolation on the main lobe of the spectrum corresponding to BHN windowing. The solid line shows the normalized continuous spectrum of a sinusoidal signal of normalized frequency $\varphi_{in} = 128.25$, the diamonds mark the bin amplitudes used as the interpolation nodes and the dashed line is the parabola fit. The difference between φ_m and φ_{in} constitutes the interpolation error.

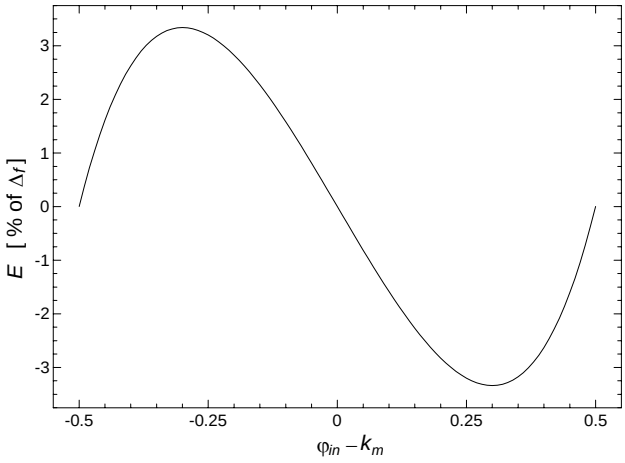

Fig. 7. Error of the parabolic interpolation on the magnitude spectrum corresponding to BHN windowing, as a percentage of the spectrum bin spacing Δ_f. The biggest error is 3.34 % for $|\varphi_{in} - k_m| \cong 0.300$.

$$E(\varphi_d) = \varphi_m - \varphi_{in} = k_m + \Delta_m - \varphi_{in} = \Delta_m - \varphi_d \tag{16}$$

where $\varphi_d = \varphi_{in} - k_m$.

As seen in **Fig. 6**, the spectrum amplitude $S[k_m - 1]$ in (10) can be expressed as

$$S[k_m - 1] = W\left(-(\varphi_d + 1)\right) = W(\varphi_d + 1) \tag{17a}$$

since the spectrum $W(\varphi)$ is an even function.

Similarly:

$$S[k_m] = W(\varphi_d) \tag{17b}$$

$$S[k_m + 1] = W(\varphi_d - 1) \tag{17c}$$

Inserting Δ_f as in (10) and equations (17a), (17b), (17c) into (16) yields

$$E(\varphi_d) = -\frac{W(\varphi_d + 1) - W(\varphi_d - 1)}{2\left(2W(\varphi_d) - W(\varphi_d + 1) - W(\varphi_d - 1)\right)} - \varphi_d \tag{18}$$

The error, expressed as a percentage of the spectrum bin spacing Δ_f, is shown in **Fig. 7** for BHN windowing within the range $\pm 0.5\ \Delta_f$ around bin k_m.

Note that equation (18) is given in the "measurement coordinate system", in which the biggest bin k_m (the interpolation center) constitutes the system origin. The continuous spectrum peak shape, as in (15), is given in the coordinate system with the peak maximum in the origin. This is the reason for negative signs in (18). For non-perturbed spectra (i.e. with no interference nor noise), the error (18) is the same around each discrete spectrum bin, i.e. is periodic with period of Δ_f.

Performance of an interpolation method can be characterized by the interpolation gain, defined as the ratio of the largest frequency error without interpolation ε given in (5), to the largest error with the interpolation

$$G = \frac{\varepsilon}{\max\left|E(\varphi_d)\right|} = \frac{\Delta_f}{2\max\left|E(\varphi_d)\right|} \tag{19}$$

Calculated in this way, a factor of 15.0 is achieved for BHN windowing and the parabolic interpolation.

The parabolic interpolation efficiencies for some other commonly known windowing methods are listed in **Table 1**. Details concerning the windows and corresponding interpolation results are given in the Appendix.

3.2. Gaussian interpolation

The frequency resolution gain achieved using the parabolic interpolation method may be further improved with a Gaussian interpolation of the discrete magnitude spectrum.

Since a Gaussian curve

$$S_g(\varphi) = \exp\left(a'(\varphi - \varphi_m)^2 + h'\right) \tag{20}$$

is a parabola in the logarithmic scale, the Gaussian interpolation reduces to the parabolic interpolation on the spectrum natural logarithm. Therefore, the Gaussian interpolation can be derived from the parabolic

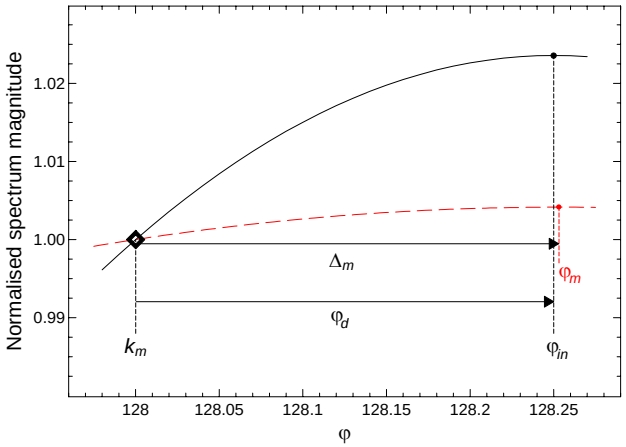

Fig. 8. Example of the Gaussian interpolation when using BHN windowing, under same conditions as in Fig. 6 (note that the figures have different scales). The solid line shows the normalized spectrum of a sinusoidal signal of frequency $\varphi_{in} = 128.25$, the diamond marks the interpolation centre bin amplitude and the dashed line is the Gaussian fit. The difference between φ_m and φ_{in} constitutes the interpolation error.

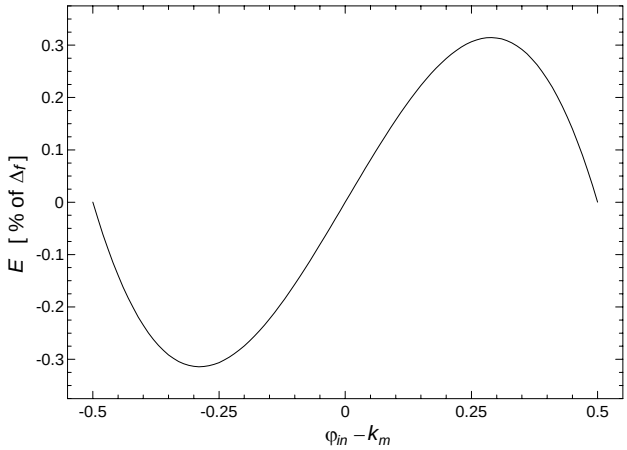

Fig. 9. Error of the Gaussian interpolation on the discrete magnitude spectrum corresponding to BHN windowing, as a percentage of the spectrum bin spacing Δ_f. The biggest error is 0.314 % for $|\varphi_{in} - k_m| \cong 0.289$.

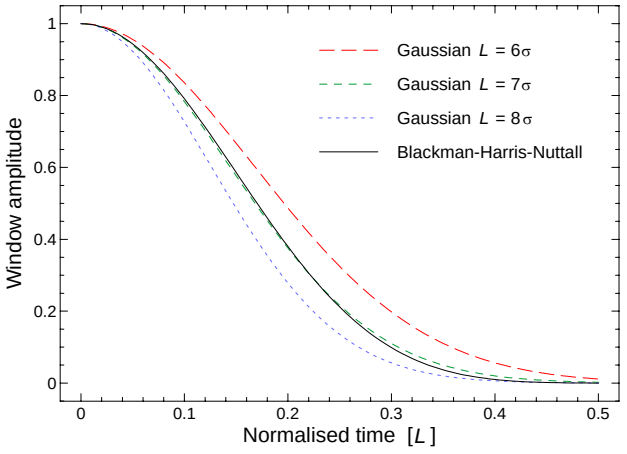

Fig. 10. Gaussian windows having widths of 6σ, 7σ and 8σ, shown together with the Blackman-Harris-Nuttall window (all the windows are symmetrical with respect to $t = 0$). Note small shape difference between the Gaussian window of 7σ and the BHN window.

interpolation (10), using the logarithmic spectrum values, i.e. instead of taking the magnitudes $S[k_m-1]$, $S[k_m]$, $S[k_m+1]$ as the interpolation nodes, one takes their natural logarithms $\ln(S[k_m-1])$, $\ln(S[k_m])$ and $\ln(S[k_m+1])$. Thus, after logarithm grouping, equation (10) becomes

$$\varphi_{in} \cong \varphi_m = k_m + \Delta_m = k_m + \frac{\ln\left(\frac{S[k_m+1]}{S[k_m-1]}\right)}{2\ln\left(\frac{S[k_m]^2}{S[k_m+1]\,S[k_m-1]}\right)} \qquad (21)$$

provided that coefficient a' in (20) is negative, which implies $S[k_m]^2 > S[k_m+1]\,S[k_m-1]$.

An example of the Gaussian interpolation with BHN windowing is shown in **Fig. 8**, under the same conditions as for the parabolic interpolation in **Fig. 6**. Note that, since the axis scales are different on each figure, the Gaussian interpolation (21) corrects most of the parabolic interpolation error.

The error of the Gaussian interpolation can be derived as for the parabolic interpolation error (18), giving

$$E(\varphi_d) = -\frac{\ln\left(\frac{W(\varphi_d+1)}{W(\varphi_d-1)}\right)}{2\ln\left(\frac{W(\varphi_d)^2}{W(\varphi_d+1)\,W(\varphi_d-1)}\right)} - \varphi_d \qquad (22)$$

for $\varphi_d = \varphi_{in} - k_m$.

The error for BHN windowing is shown in **Fig. 9** as a percentage of the spectrum bin spacing Δ_f. The gain factor (19) is calculated to be 159.

The Gaussian interpolation gain can be enhanced further by using Gaussian windowing. Let $w_{gau}(t)$ be a Gaussian window of standard deviation σ and length L, which is cut symmetrically at time values $-L/2$ and $L/2$. The window has the form

$$w_{gau}(t) = w_r(t)\exp\left(-\frac{t^2}{2\sigma^2}\right) \qquad (23)$$

where $w_r(t)$ is the rectangular window (11).

Figure 10 shows three Gaussian windows of length L of 6σ (i.e. the Gaussian curve is cut at -3σ and 3σ), 7σ and 8σ. Notice that the BHN window, which is presented for a comparison, is very similar to the Gaussian window of 7σ.

If a Gaussian window (23) is applied to a sinusoidal signal of frequency f_{in}, then the spectrum of the resultant signal has a local maximum at f_{in} and its shape, corresponding to the Fourier transform of the window has been calculated as

$$W_{gau}(\varphi_o) = \sqrt{\frac{\pi}{2}}\,\rho\exp\left(-2\pi^2\rho^2{\varphi_o}^2\right)\cdot \left|\operatorname{erf}\left(\frac{1+\mathrm{j}\,4\pi\rho^2\varphi_o}{2\sqrt{2}\,\rho}\right)+\operatorname{erf}\left(\frac{1-\mathrm{j}\,4\pi\rho^2\varphi_o}{2\sqrt{2}\,\rho}\right)\right| \qquad (24)$$

where $\varphi_o = \varphi - \varphi_{in}$, $\varphi = Lf$, $\rho = \sigma/L$ and erf() is the error function, generalized for a complex argument.

The spectrum magnitude (24) is shown for windows of $L = 6\sigma$, $L = 7\sigma$ and $L = 8\sigma$ in **Fig. 11a**, **12a** and **13a** respectively.

Note that, as listed in **Table 1**, spectral properties of Gaussian windows are inferior to the Blackman-Harris-Nuttall one. For the Gaussian window of length 6σ the spectrum main lobe is narrower, but the sidelobes are 36 dB higher than for the BHN window. When making the Gaussian windows steeper, the sidelobes get smaller at the expense of substantial widening of the main lobe, but they do not reach the level of the BHN window even for the Gaussian window of 8σ, which is much steeper

Table 1. Efficiency of the parabolic and Gaussian interpolation with different windowing methods. The windows are characterised by main lobe width, highest sidelobe level and sidelobe asymptotic fall-off. The maximum interpolation error is given as a percentage of the spectrum bin spacing Δ_f. The interpolation gain factor G is defined in (19). Some details concerning the windows and the interpolation errors are given in the Appendix.

Window	Main lobe width [bin]	Highest sidelobe [dB]	Sidelobe asymptotic fall-off [dB/oct]	**Parabolic interpolation**		**Gaussian interpolation**	
				Error max. [% of Δ_f]	**Gain factor G**	**Error max. [% of Δ_f]**	**Gain factor G**
Rectangular	2	-13.3	6	23.4	2.14	16.7	2.99
Triangular	4	-26.5	12	6.92	7.23	2.08	24.1
Hann	4	-31.5	18	5.28	9.47	1.60	31.2
Hamming	4	-44.0	6	6.80	7.35	1.60	31.2
Blackman	6	-68.2	6	4.66	10.7	0.578	86.5
Blackman-Harris	6.54	-74.4	6	4.18	12.0	0.476	105
Nuttall	8	-98.2	6	3.51	14.2	0.314	159
Blackman-Harris-Nuttall	8	-93.3	18	3.34	15.0	0.314	159
Gaussian $L = 6\,\sigma$	6.96	-57.2	6	4.95	10.1	0.240	208
Gaussian $L = 7\,\sigma$	10.46	-71.0	6	3.80	13.2	0.0516	970
Gaussian $L = 8\,\sigma$	11.41	-87.6	6	2.95	17.0	0.00869	5756

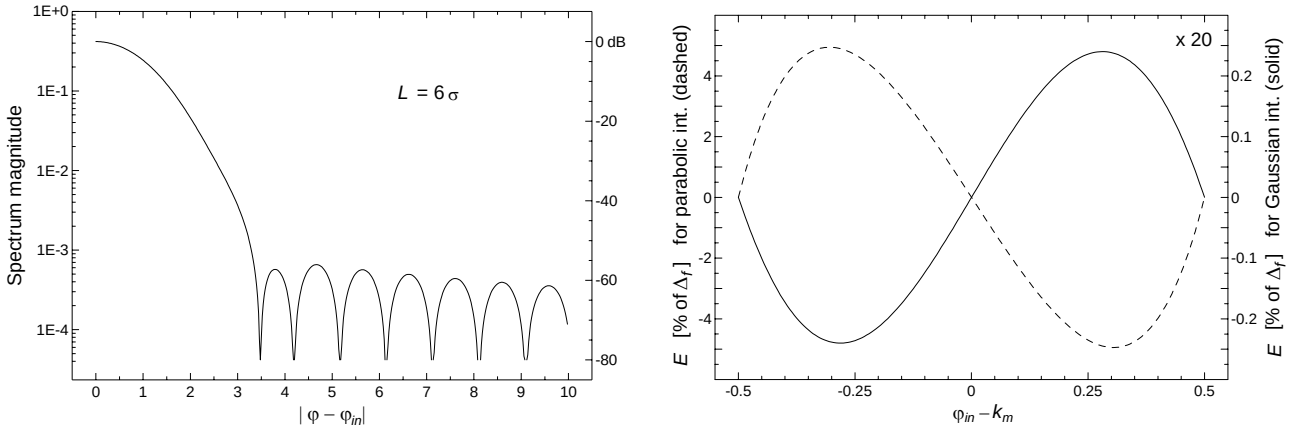

a) b)

Fig. 11. Gaussian windowing for $L = 6\sigma$. Figure a) shows the magnitude spectrum around its maximum at φ_{in}. The right vertical axis is scaled in dB referred to 0.417, the main lobe maximum. Figure b) presents the interpolation errors. The biggest parabolic interpolation error is 4.95 % of Δ_f for $|\varphi_{in} - k_m| \cong 0.305$ (the dashed line and left vertical axis). The biggest Gaussian interpolation error is 0.240 % of Δ_f for $|\varphi_{in} - k_m| \cong 0.282$ (the solid line and right vertical axis scaled up 20 times).

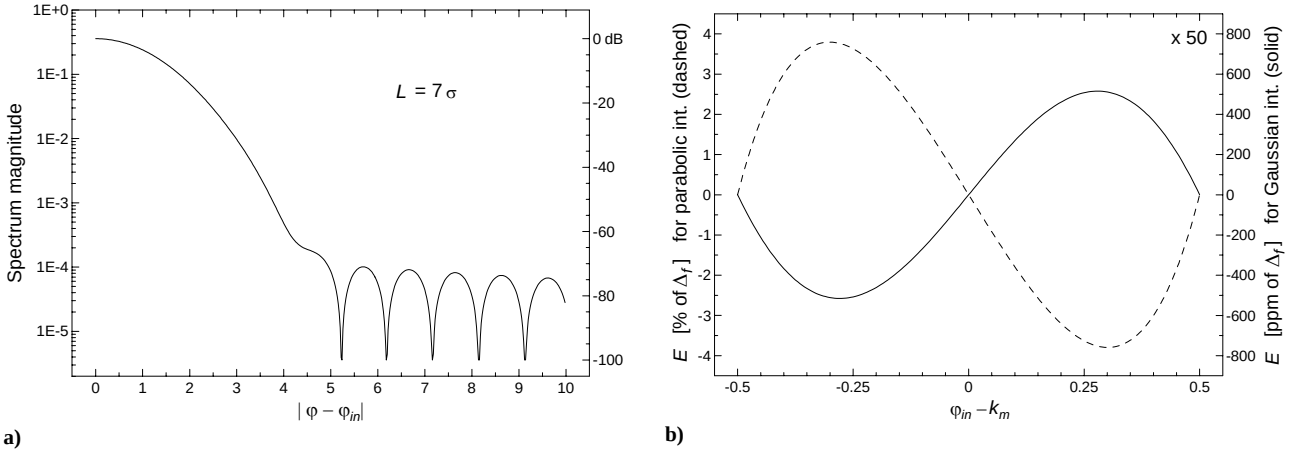

a) b)

Fig. 12. Gaussian windowing for $L = 7\sigma$. Figure a) shows the magnitude spectrum around its maximum at φ_{in}. The right vertical axis is scaled in dB referred to 0.358, the main lobe maximum. Figure b) presents the interpolation errors. The biggest parabolic interpolation error is 3.80 % of Δ_f for $|\varphi_{in} - k_m| \cong 0.301$ (the dashed line and left vertical axis). The biggest Gaussian interpolation error is 516 ppm of Δ_f for $|\varphi_{in} - k_m| \cong 0.279$ (the solid line and right vertical scaled up 50 times).

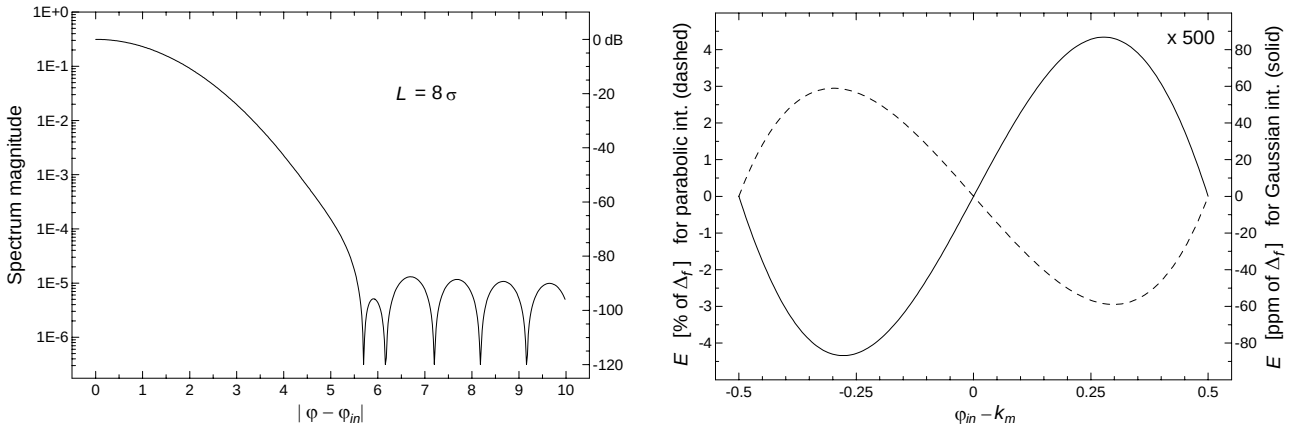

a) b)

Fig. 13. Gaussian windowing for $L = 8\sigma$. Figure a) shows the magnitude spectrum around its maximum at φ_{in}. The right vertical axis is scaled in dB, referred to 0.313, the main lobe maximum. Figure b) presents the interpolation errors. The biggest parabolic interpolation error is 2.95 % of Δ_f for $|\varphi_{in} - k_m| \cong 0.298$ (the dashed line and left vertical axis). The biggest Gaussian interpolation error is 86.9 ppm of Δ_f for $|\varphi_{in} - k_m| \cong$ of 0.278 (the solid line and right vertical axis scaled up 500 times).

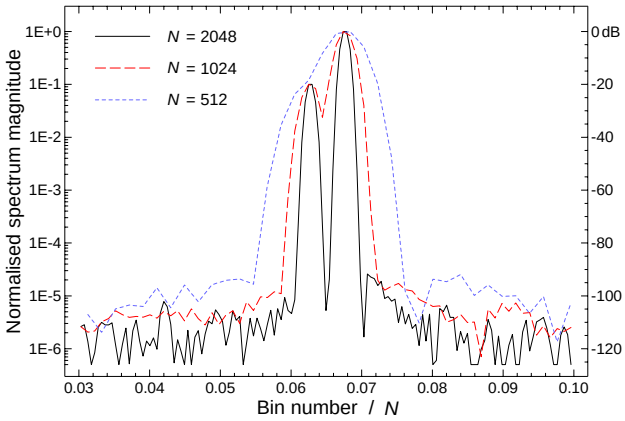

Fig. 14. Parts of spectra of simulated signals, scaled and rounded to 14-bit full-scale samples. Each signal has two sinusoidal components. The lower frequency component (signal of interest), has an amplitude 10 times smaller than that of the second one (interference). The component frequency pairs are: $\varphi_1 = 128.5$ and $\varphi_2 = 138.5$ for $N = 2048$, $\varphi_1 = 64.25$ and $\varphi_2 = 69.25$ for $N = 1024$, $\varphi_1 = 32.125$ and $\varphi_2 = 34.625$ for $N = 512$. These numbers were chosen to keep the same signal to clock frequency ratio for all N, to show all spectra in the same scale. When N decreases, the peaks gradually merge and noise level increases.

than the BHN one. Also, the sidelobe asymptotic decay of Gaussian windowing is only 6 dB per octave, while the BHN windowing gives three times higher fall-off.

Although spectral properties of Gaussian windows are not optimal, these windows give spectra with main lobe shapes very close to the Gaussian form, which can be interpolated using (21) with particularly small error. Error (22) of the Gaussian interpolation is shown in **Fig. 11b**, **12b** and **13b** for Gaussian windows of length of 6σ, 7σ and 8σ respectively. For comparison, the error of the parabolic interpolation, calculated using equation (18), is also plotted. Notice large disparities in scales for the parabolic and Gaussian interpolation errors, respectively of 20, 50 and 500 times. The gain factor (19) for the Gaussian interpolation with Gaussian windows of length of 6σ, 7σ and 8σ is calculated to be 208, 970 and 5756 respectively.

The yields of the Gaussian interpolation are listed in **Table 1** for a few other commonly known windowing methods. Some details concerning the windows and corresponding interpolation results are given in the Appendix.

Since spectrum interpolation can improve frequency measurement resolution by orders of magnitude, one could think that it is possible to reduce the number of signal samples by similar factor, keeping the resolution as without interpolation. Such a conclusion is true only to some extent, because prior to applying one of the described interpolation methods, the local maximum of the magnitude spectrum has to be found. That implies resolving nearby spectrum peaks, which is only possible when spectrum bin spacing is small enough to ensure that the lobes corresponding to those peaks do not merge.

As an example, **Fig. 14** shows parts of discrete spectra of three similar signals that were simulated to get different spectrum bin spacing. Each signal, simulated as 14-bit full-scale samples, has two sinusoidal components, seen as two spectral peaks. The component of lower frequency, which is the target, has 10 times smaller amplitude than the second one, simulating a strong nearby interference. The signal and clock frequencies were chosen to present spectra on the same scale, i.e. the ratios of the component to clock frequencies were constant. When the spectrum has 2048 points (solid line), both peaks are well separated. On the spectrum with 1024 points (long-dashed line) the peaks start overlapping, but the smaller peak can still be detected and the frequency of the corresponding component can be calculated using spectrum interpolation. Further data reduction to 512 samples (short-dashed line), causes both peaks to merge and the smaller peak cannot be found any more. Assuming that this particular example shows the worst measurement case (the signal has the lowest amplitude, the interference is the largest and the distance between them is the smallest ever possible), the FFT size can be chosen as 1024 points.

For other conditions, the minimum number of samples could be different. It is important indeed to choose the number of samples to guarantee sufficient bin spacing for any measured signal, taking into account the worst-case conditions.

To perform precise interpolation, the node values should be known with sufficient accuracy. Since the node values are biased by noise, accurate interpolation may need high signal-to-noise ratio (SNR) of the discrete spectrum, which depends on the noise already present in the analyzed signal and the noise introduced by an analogue-to-digital converter (ADC) (in the ideal case it is only the quantization noise, but usually the converter introduces also some other noise). The noise floor in the discrete spectrum as well is contingent upon the number of FFT points. The noise can be lowered by increasing the FFT size (property of the FFT, seen in Fig. 14 as the smaller noise level for the larger FFT size).

Note that the widths of spectral peaks as well as noise properties, obtained with FFT analysis, depend on the window applied to the input samples **[7]**. For that reason, the windowing method affects not only the frequency resolution gain given by spectrum interpolation, but also the number of FFT points guaranteeing reliable frequency measurements.

4. Measurements

The parabolic and Gaussian interpolation methods were examined with a laboratory test set-up. A sine signal of precisely known frequency was introduced to an input of an FFT-based frequency measurement system. The system, utilizing either parabolic or Gaussian interpolation, measured the frequency, which was compared with the actual frequency of the input signal.

The laboratory set-up, shown schematically in **Fig. 15**, was part of a tune measurement development system **[6]**. It consisted of an analogue channel with a 14-bit ADC, a memory for fast ADC sample storage, and a board with a floating-point digital signal processor (DSP). A PC was used to prepare processing software and to download it to the DSP board, via a dedicated interface card.

If the input signal frequency changes during acquisition, the FFT frequency measurements reflect that,

unlike classical counting methods. For that reason, the phase stability of the input and clock signal sources was crucial. Since it was very difficult to find frequency generators stable enough for these measurements, both input and clock frequencies were produced using two direct digital synthesizers (DDSs), driven by the reference oscillator of a frequency meter. Because it was the ratio of these frequencies that was measured (see equation (4)), the phase stability of the reference generator was less critical. The ratio was fixed with very good precision by DDS settings and the frequency meter was used only for testing purposes.

During each acquisition, 2048 ADC samples of the sine wave input signal were stored in memory. Then, the DSP successively performed the BHN or Gaussian windowing, the FFT and the power spectrum calculation. Next, the spectrum bin with the biggest amplitude was found and finally the input frequency was calculated according to (10) or (21).

Even when using a single reference oscillator and two DDSs, consecutive measurements gave slightly different results for the same setup frequencies. To reflect this, 100 measurements were performed and the resulting two extreme values collected. The measurements were done around bin 128 [(1)], for normalized frequency $\varphi = f N T_s$ ranging from 127.5 to 128.5. For the ADC clock of 1.25 MHz the input frequency was about 78 kHz (mid-range of the frequency span of the tune measurement system). To minimize system noise influence on the measurement accuracy, the signal amplitude was close to the ADC full scale.

Measurement errors of the parabolic and Gaussian interpolation with BHN windowing are presented in **Fig. 16** and **17** respectively. The errors are calculated as the difference between the frequency computed by the system and the input frequency set by the DDS. The crosses mark both extreme values from 100 measurements (in **Fig. 16** the error uncertainty is so small that both crosses overlap). The expected errors, calculated with equations (18) or (22), are also plotted with dashed lines.

Without interpolation the frequency measurement error would be 50 % of the bin spacing Δ_f. Using the parabolic or Gaussian interpolation, the theoretical error can be respectively reduced by a factor of 15 (to 3.3 % of Δ_f) or 159 (to 0.31 % of Δ_f). The measurements yielded very similar values.

To investigate the limits of the Gaussian interpolation, measurements were done also with Gaussian windowing. Corresponding interpolation errors for Gaussian windows of 7σ and 8σ respective lengths are shown in **Fig**. **18** and **19**. In this case the uncertainty of the frequency measurement error gets more visible, since the error is much smaller than in **Fig**. **16** and **17**.

Using the Gaussian interpolation with Gaussian windowing of 7σ, the theoretical error can be reduced by a factor of 970 (to 516 ppm of Δ_f). The measurements gave a factor of 936 (to 534 ppm of Δ_f). For Gaussian windowing of 8σ, the theoretical reduction is a factor of 5756 (to 87 ppm of Δ_f). The measurements yielded a factor of 4682 (the error decreased to 107 ppm of Δ_f).

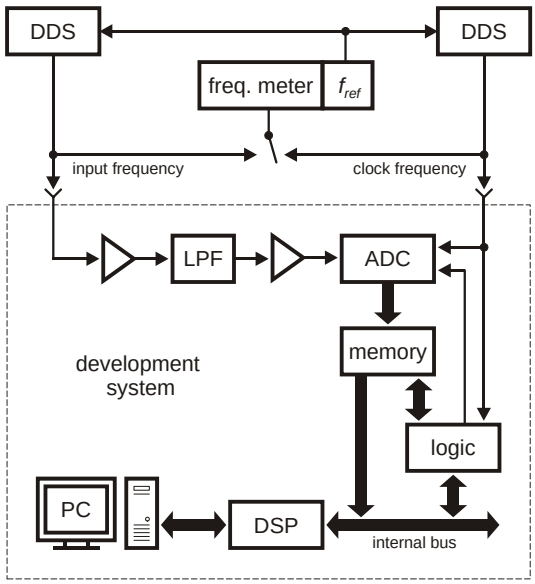

Fig. 15. The measurement set-up used to examine the interpolation methods. The items inside the dashed line rectangle form a tune development system **[5]**. The direct digital synthesisers (DDS) produce the input and clock frequencies from a stable quartz oscillator (10 MHz reference from HP8656A). The low-pass filter (LPF) works as an antialias filter.

For Gaussian windowing, the measurement errors were significantly worse than the theoretical ones. The errors from measurements were so small that they were already affected by noise, believed to originate in the analogue channel likely with the largest contribution from the DDS output 12-bit digital-to-analogue converter. This amplitude noise was converted into frequency error during the interpolation process. Other possible contributions are quantization noise of the ADC and an uncertainty caused by a finite accuracy of the DSP arithmetic (single precision floating point numbers IEEE 754-1985, having an accuracy of about 0.1 ppm).

Notice that the measurement error of 107 ppm of the bin spacing gives the relative error of 0.8 ppm when referred to bin 128, and of 0.1 ppm when referred to bin 1024, which corresponds to the highest theoretical frequency that could be processed (Nyquist frequency). These values are very close to the DSP arithmetic limit, despite the fact that the final value was the result of many operations, namely windowing, FFT, module calculation and interpolation.

It is worth noting that the interpolation gain factor of 4682, as obtained from the measurements at the expense of performing the Gaussian interpolation (21) within some microseconds, is equivalent to multiplying both the number of input signal samples and the sampling time for standard FFT measurement by this factor. For the presented measurements, it means increasing the number of samples from 2048 to some 9 500 000 and the sampling time from 1.6 ms to 7.5 s. Such an amount of data would multiply the FFT calculation time by a factor of 9870 [(2)], from about 2 ms to some 20 s.

[(1)] An arbitrary choice of a bin around which measurements are done does not influence the error results as long as they are expressed in units of Δ_f.

[(2)] $\frac{4682 \cdot 2048 \cdot \log_2(4682 \cdot 2048)}{2048 \cdot \log_2(2048)} \approx 9870$

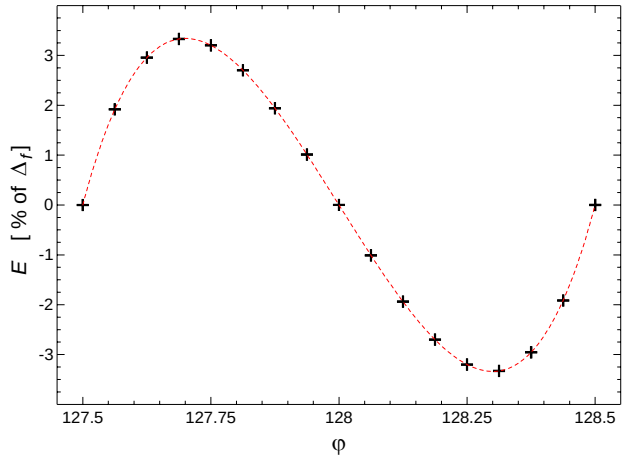

Fig. 16. Measurement error for the parabolic interpolation and BHN windowing, as a percentage of the bin spacing Δ_f. The crosses mark extreme values from 100 consecutive measurements (in this case the error uncertainty is so small that both crosses overlap) and the dashed line gives the theoretical error (18). The biggest measurement error is the same as the theoretical one (3.3 %).

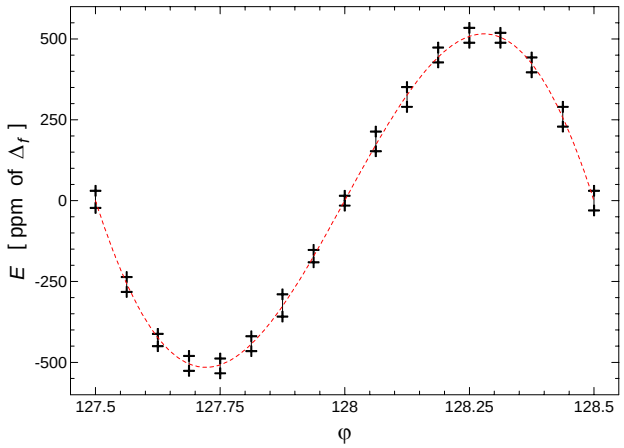

Fig. 18. Measurement error for the Gaussian interpolation and Gaussian windowing with $L = 7\sigma$, as ppm of the bin spacing Δ_f. The crosses mark extreme values from 100 consecutive measurements and the dashed line gives the theoretical error (22). The biggest measurement error is 534 ppm, similar to the theoretical one (516 ppm).

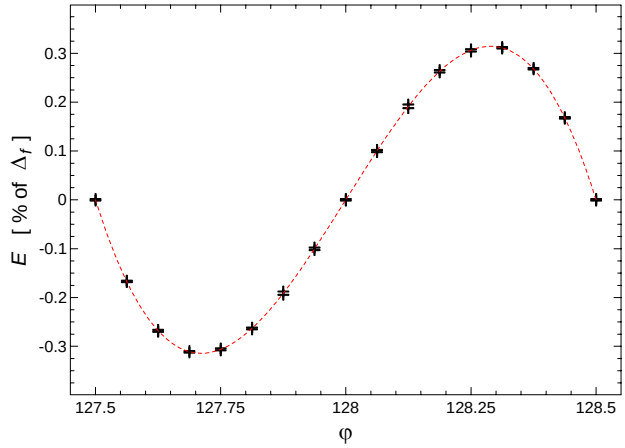

Fig. 17. Measurement error for the Gaussian interpolation and BHN windowing, as a percentage of the bin spacing Δ_f. The crosses mark extreme values from 100 consecutive measurements and the dashed line gives the theoretical error (22). The biggest measurement error is very close to the theoretical one (0.31 %).

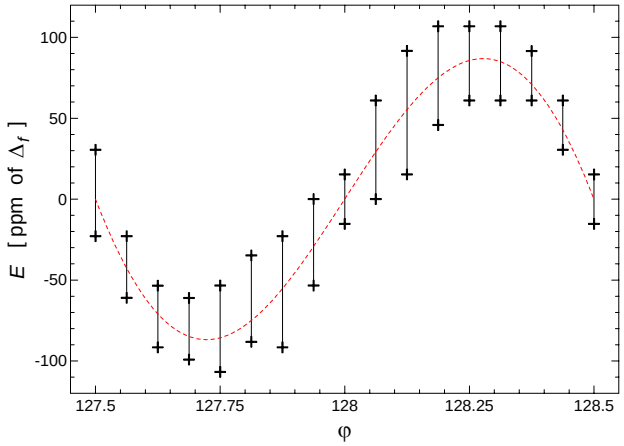

Fig. 19. Measurement error for the Gaussian interpolation and Gaussian windowing with $L = 8\sigma$, as ppm of the bin spacing Δ_f. The crosses mark extreme values from 100 consecutive measurements and the dashed line gives the theoretical error (22). The biggest measurement error is 107 ppm, larger than the theoretical one (87 ppm).

5. Conclusions

Theoretical and experimental studies have been undertaken to enhance FFT frequency measurement resolution, using parabolic or Gaussian interpolation on the discrete magnitude spectrum. For both methods the interpolation yield strongly depends upon the windowing method used.

While parabolic interpolation can improve the frequency resolution by more than one order of magnitude, this paper has shown that the interpolation gain can still get better with Gaussian interpolation. An improvement larger than two orders of magnitude is achievable with windows having very good spectral properties and well beyond three orders of magnitude when using steep Gaussian windows. Theoretical results have been proved by laboratory measurements.

The FFT size cannot be directly determined from the frequency resolution gain achieved with interpolation due to the fact that to resolve nearby spectrum peaks bin spacing should be small enough to avoid peak merging.

Gaussian interpolation can favorably replace the parabolic method used in the tune measurement systems for the CERN Proton Synchrotron Booster (PSB) and Proton Synchrotron (PS) accelerators **[6]**. Since the FFT size was chosen to get sufficient frequency resolution with the parabolic interpolation, that size could be reduced using the Gaussian method, with an order of magnitude better interpolation gain. That would decrease calculation time, achieve still better frequency resolution and allow tune measurements, for both horizontal and vertical planes, at least every 5 ms, instead of 10 ms as in the present system.

6. Acknowledgements

The authors are indebted to all those involved in the development of the tune measurement system for the PSB accelerator. A special mention is given to E.T. d'Amico and A. Chapman-Hatchett. The authors also thank J. Belleman, J. Bosser, J.P. Potier and U. Raich for the many valuable remarks.

7. References

[1] A. Chapman-Hatchett, V. Chohan, E.T. d'Amico, *Tune measurement for the CERN Proton Synchrotron Booster rings using DSP in VME.* CERN/PS 99-031 (BD). Particle Accelerator Conference, New York, USA, March 29-April 2, 1999.

[2] E. Asséo, *Causes et corrections des erreurs dans la mesure des caractéristiques des oscillations bétatroniques obtenues à partir d'une Transformation de Fourier*, CERN PS 85-9 (LEA), December 1985.

[3] J. Gonzalez, S. Johnston, E. Schulte, *Fast Q-measurement for the PS by FFT analysis.* CERN/PS 94-1 (BD). European Particle Accelerator Conference, London, UK, June 23-July 1, 1994.

[4] R. Bartolini, A. Bazzani, M. Giovannozzi, W. Scandale, E. Todesco, *Tune evaluation in simulations and experiments*. CERN/SL 95-84 (AP), 1995.

[5] R. Bartolini, M. Giovannozzi, W. Scandale, E. Todesco, *Algorithms for a precise determination of the betatron tune*. CERN/SL 96-48 (AP). Proceedings of the 5-th European Particle Accelerator Conference EPAC96, Sitges, Spain, Vol. II, (1996), pp. 1329-1331.

[6] M. Gasior, J.L. Gonzalez, *DSP Software of the Tune Measurement System for the Proton Synchrotron Booster Accelerator*. CERN/PS/BD Note 99-11, September 1999.

[7] F.J. Harris, *On the Use of Windows for Harmonic Analysis with the Discrete Fourier Transform*, Proceedings of the IEEE, Vol. 66, No. 1, January 1978, pp. 51-83.

[8] A.H. Nuttall, *Some Windows with Very Good Sidelobe Behavior.* IEEE Transactions on Acoustics, Speech, and Signal Processing, Vol. ASSP-29, No. 1, February 1981, pp. 84-91.

Appendix

Interpolation of discrete magnitude spectra using other windows

A.1. Summary

Detailed results of the parabolic and Gaussian interpolation methods have been shown, when used with Blackman-Harris-Nuttall **[8]** and Gaussian windowing. In this appendix some corresponding results are presented for a few other commonly known windows.

Shapes of the rectangular and BHN windows, as described in the paper, are shown in **Fig. A-1** alongside with six other windows **[7]**: triangular, Hann, Hamming, Blackman, Blackman-Harris and Nuttall. The interpolation errors resulting from their application are presented in the following sections.

A.2. Rectangular windowing

As discussed in section 3.1, the rectangular window is not suitable for three-node interpolation. It is considered here only to allow comparisons of interpolation result with other windows.

The main sidelobe of the rectangular windowing spectrum (13) (see **Fig. 3**) has a width of 2 bins. Since the main lobe is too narrow (it must be at least 3 bins), the three-node interpolation extends to either the adjacent lower or higher sidelobe, depending upon whether the maximum bin of the discrete spectrum is located below or above the input frequency. That explains why the interpolation efficiencies are so poor for this windowing. Note that the spectral leakage is large, since the first sidelobe is only 13.3 dB below the main lobe.

The errors of the parabolic and Gaussian interpolation with rectangular windowing, calculated from (18) and (22) respectively, are shown in **Fig. A-2**.

A.3. Triangular windowing

The triangular window is probably the simplest that allows an efficient three-node interpolation on discrete magnitude spectrum peaks. The window is defined as

$$w_{trg}(t) = w_r(t)\left(1 - 2\left|\frac{t}{L}\right|\right) \qquad \text{(A-1)}$$

where $w_r(t)$ is the rectangular window (11) and L is the window length.

The corresponding magnitude spectrum, plotted in **Fig. A-3a**, has been found as

$$W_{trg}(\varphi_o) = \frac{1}{2}\left|\frac{\sin\left(\frac{1}{2}\pi\varphi_o\right)}{\frac{1}{2}\pi\varphi_o}\right|^2 \qquad \text{(A-2)}$$

where $\varphi_o = \varphi - \varphi_{in}$ and φ_{in} is the normalized frequency of the sinusoidal component, which the spectrum peak corresponds to.

The main lobe width is four bins and, as such, is sufficient for the three-node interpolation. Note that the first sidelobe is considerably lower than that of the rectangular window (see **Table 1** for details).

The errors of the parabolic and Gaussian interpolation with triangular windowing, calculated according to (18) and (22) respectively, are shown in **Fig. A-3b**. Since the main lobe is wide enough for the interpolation, the errors are much smaller than those corresponding to rectangular windowing.

A.4. Hann windowing

The Hann window is defined as

$$w_{han}(t) = w_r(t)\left[\frac{1}{2} + \frac{1}{2}\cos\left(\frac{2\pi}{L}t\right)\right] \qquad \text{(A-3)}$$

The corresponding magnitude spectrum, plotted in **Fig. A-4a**, is

$$W_{han}(\varphi_o) = \left|\frac{\sin(\pi\varphi_o)}{2\pi\varphi_o}\,\frac{1}{1-\varphi_o^2}\right| \qquad \text{(A-4)}$$

The Hann windowing sidelobes are smaller than those of triangular windowing and they fall off faster because, for large φ_o, $W_{han}(\varphi_o) \propto \varphi_o^{-3}$ and $W_{trg}(\varphi_o) \propto \varphi_o^{-2}$. See **Table 1** for details.

The errors of the parabolic and Gaussian interpolation with Hann windowing, calculated according to (18) and (22) respectively, are shown in **Fig. A-4b**.

A.5. Hamming windowing

The Hamming window is defined as

$$w_{ham}(t) = w_r(t)\left[0.54 + 0.46\cos\left(\frac{2\pi}{L}t\right)\right] \qquad \text{(A-5)}$$

The corresponding magnitude spectrum, plotted in **Fig. A-5a**, has the form of

$$W_{ham}(\varphi_o) = \left|\left(0.08\varphi_o^2 - 0.54\right)\frac{\sin(\pi\varphi_o)}{\pi\varphi_o}\,\frac{1}{\varphi_o^2 - 1}\right| \qquad \text{(A-6)}$$

Unlike the Hann window, the Hamming window does not fall off to zero on its boundaries (see **Fig. A-1**). Nevertheless, the biggest sidelobe of the corresponding spectrum is smaller than that of Hann windowing. On the other hand, sidelobes fall off faster for Hann than for Hamming windowing. See **Table 1** for details.

The errors of the parabolic and Gaussian interpolation with Hamming windowing, calculated according to (18) and (22) respectively, are shown in **Fig. A-5b**. The errors are similar to those of Hann windowing, even though there are significant differences in spectrum shapes, including main lobes.

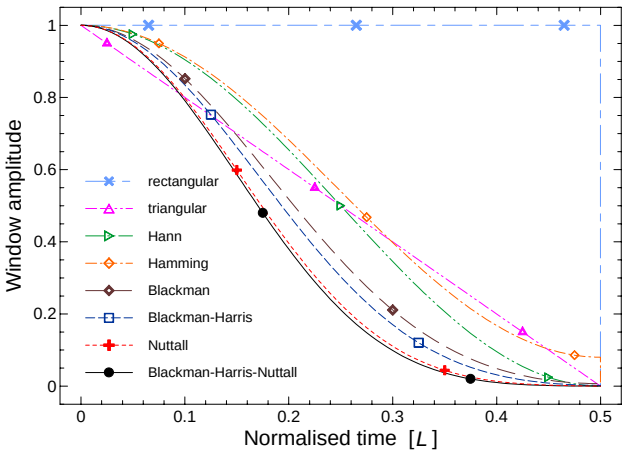

Fig. A-1. Shapes of the windows reviewed in **Table 1**, excluding Gaussian windows, already shown in **Fig. 10**. The windows are symmetrical with respect to $t = 0$. They are defined in the appendix, except for the rectangular and BHN windows, specified already in (11) and (14) respectively.

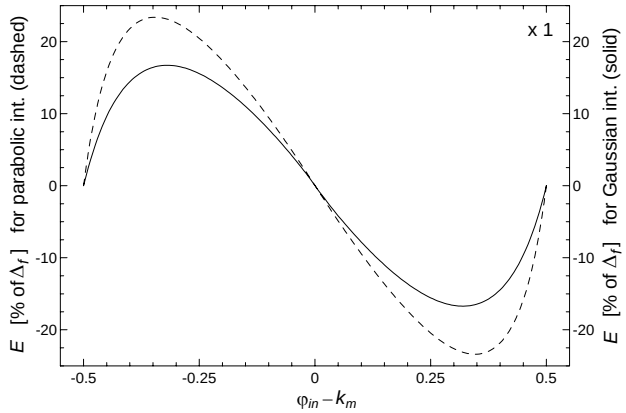

Fig. A-2. Rectangular windowing. Interpolation error as a percentage of the spectrum bin spacing Δ_f. For the parabolic interpolation (the dashed line and left vertical axis) the biggest error is 23.4 % at a displacement $|\varphi_0 - k_m| \cong 0.346$. For the Gaussian interpolation (the solid line and right vertical axis) the biggest error is 16.7 % at a displacement $|\varphi_0 - k_m| \cong 0.319$.

A.6. Blackman windowing

The (so called exact) Blackman window is defined as

$$w_{bkm}(t) = w_r(t)\sum_{i=0}^{2} c_i \cos\left(\frac{2\pi i}{L}t\right) \qquad \text{(A-7)}$$

where $c_0 = \frac{7938}{18608}$, $c_1 = \frac{9240}{18608}$, $c_2 = \frac{1430}{18608}$.

The corresponding magnitude spectrum, presented in **Fig. A-6a**, has the form of

$$W_{bkm}(\varphi_o) = \left|\frac{\varphi_d}{\pi}\sin(\pi\varphi_o)\sum_{i=0}^{2}\frac{(-1)^i c_i}{\varphi_o{}^2 - i^2}\right| \qquad \text{(A-8)}$$

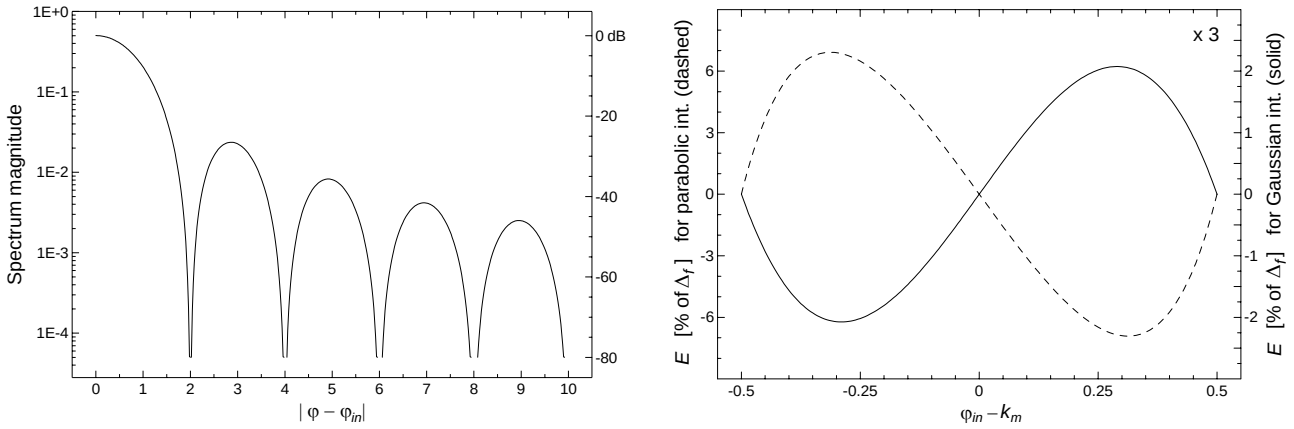

a) **b)**

Fig. A-3. Triangular windowing. Figure a) shows the magnitude spectrum around its maximum at φ_{in}. The right vertical axis is scaled in dB referred to 0.500, the main lobe maximum. Figure b) presents the interpolation errors. The biggest parabolic interpolation error is 6.92 % of Δ_f for $|\varphi_{in} - k_m| \cong 0.312$ (the dashed line and left vertical axis). The biggest Gaussian interpolation error is 2.08 % of Δ_f at $|\varphi_{in} - k_m| \cong 0.290$ (the solid line and right vertical axis scaled up 3 times).

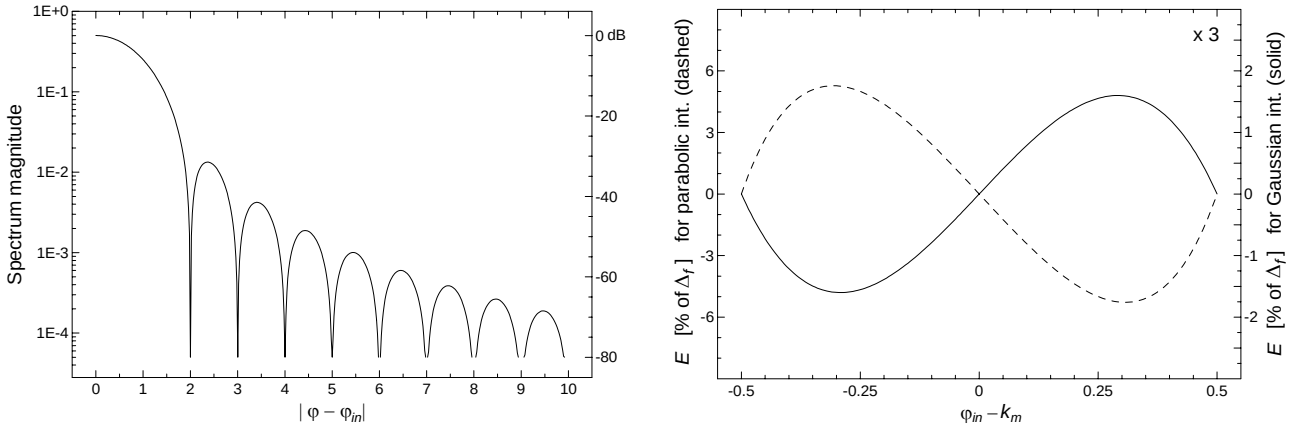

a) **b)**

Fig. A-4. Hann windowing. Figure a) shows the magnitude spectrum around its maximum at φ_{in}. The right vertical axis is scaled in dB referred to 0.500, the main lobe maximum. Figure b) presents the interpolation errors. The biggest parabolic interpolation error is 5.28 % of Δ_f for $|\varphi_{in} - k_m| \cong 0.307$ (the dashed line and left vertical axis). The biggest Gaussian interpolation error is 1.60 % of Δ_f for $|\varphi_{in} - k_m| \cong 0.291$ (the solid line and right vertical axis scaled up 3 times).

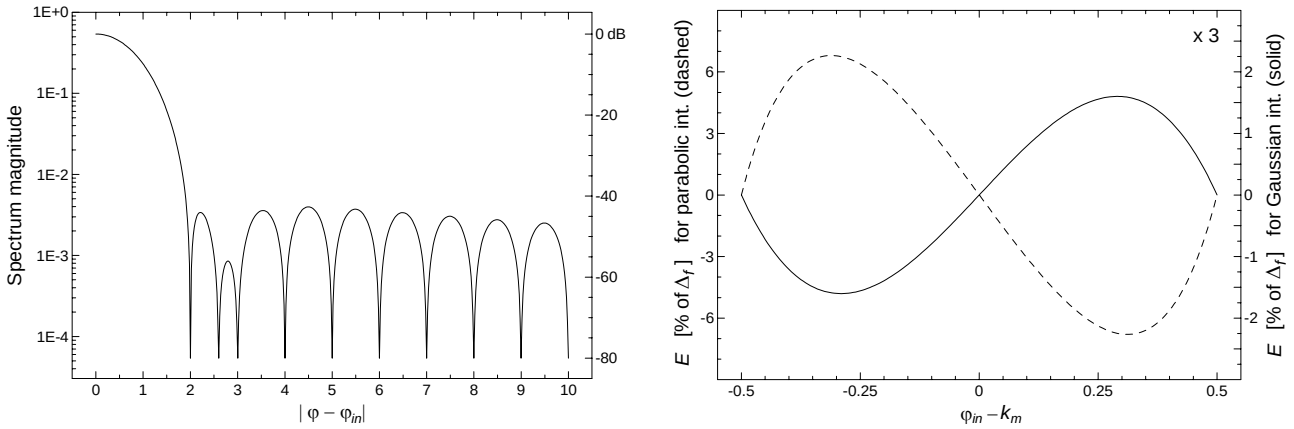

a) **b)**

Fig. A-5. Hamming windowing. Figure a) shows the magnitude spectrum around its maximum at φ_{in}. The right vertical axis is scaled in dB referred to 0.540, the main lobe maximum. Figure b) presents the interpolation errors. The biggest parabolic interpolation error is 6.80 % of Δ_f for $|\varphi_0 - k_m| \cong 0.311$ (the dashed line and left vertical axis). The biggest Gaussian interpolation error is 1.60 % of Δ_f for $|\varphi_0 - k_m| \cong 0.290$ (the solid line and right vertical axis scaled up 3 times).

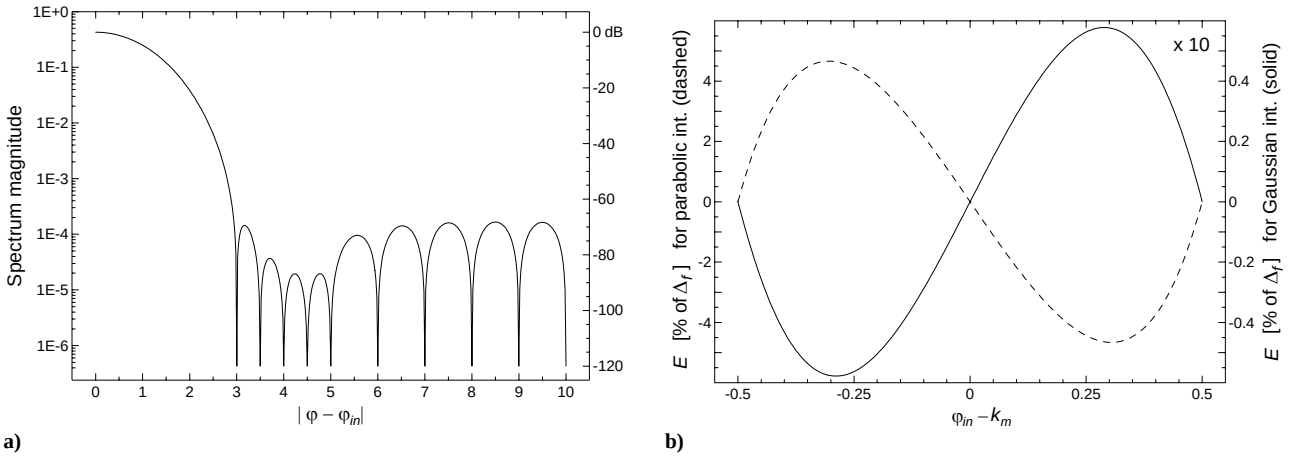

a) **b)**

Fig. A-6. Blackman windowing. Figure a) shows the magnitude spectrum around its maximum at φ_{in}. The right vertical axis is scaled in dB referred to 0.427, the main lobe maximum. Figure b) presents the interpolation errors. The biggest parabolic interpolation error is 4.66 % of Δ_f for $|\varphi_{in} - k_m| \cong 0.304$ (the dashed line and left vertical axis). The biggest Gaussian interpolation error is 0.578 % of Δ_f for $|\varphi_{in} - k_m| \cong 0.289$ (the solid line and right vertical axis scaled up 10 times).

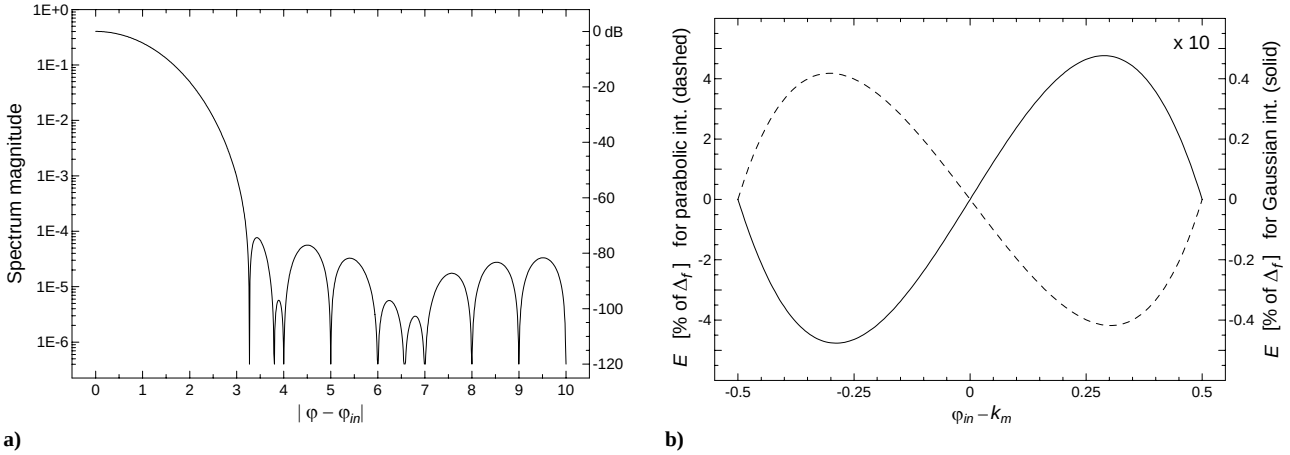

a) **b)**

Fig. A-7. Blackman-Harris windowing. Figure a) shows the magnitude spectrum around its maximum at φ_{in}. The right vertical axis is scaled in dB referred to 0.402, the main lobe maximum. Figure b) presents the interpolation errors. The biggest parabolic interpolation error is 4.18 % of Δ_f for $|\varphi_{in} - k_m| \cong 0.303$ (the dashed line and left vertical axis). The biggest Gaussian interpolation error is 0.476 % of Δ_f for $|\varphi_{in} - k_m| \cong 0.289$ (the solid line and right vertical axis scaled up 10 times).

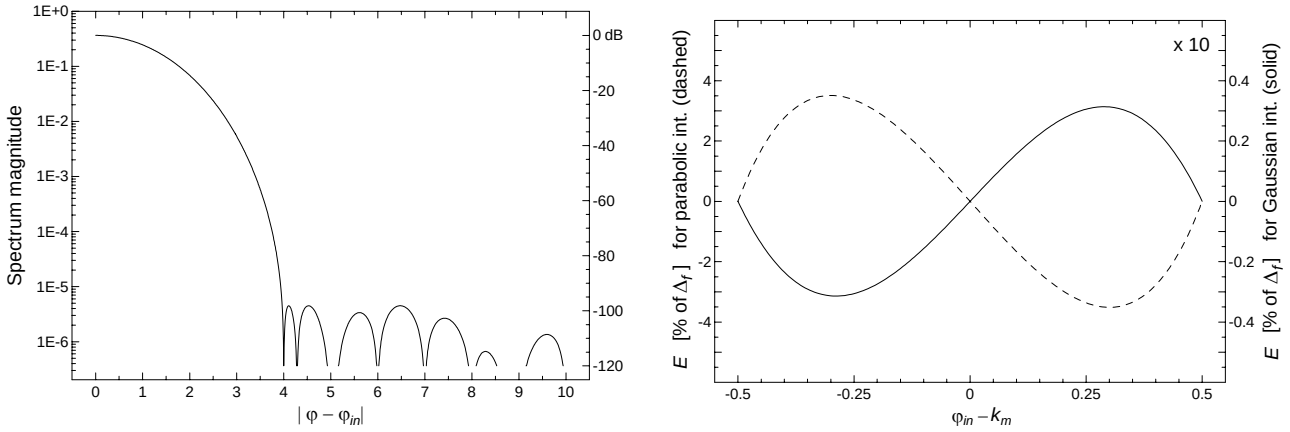

a) **b)**

Fig. A-8. Nuttall windowing. Figure a) shows the magnitude spectrum around its maximum at φ_{in}. The right vertical axis is scaled in dB referred to 0.364, the main lobe maximum. Figure b) presents the interpolation errors. The biggest parabolic interpolation error is 3.51 % of Δ_f for $|\varphi_{in} - k_m| \cong 0.300$ (the dashed line and left vertical axis). The biggest Gaussian interpolation error is 0.314 % of Δ_f for $|\varphi_{in} - k_m| \cong 0.289$ (the solid line and right vertical axis scaled up 10 times).

Adding the third cosine term to the window shape reduces the largest sidelobe level significantly. See **Table 1** for details.

The errors of the parabolic and Gaussian interpolation with Blackman windowing, calculated according to (18) and (22) respectively, are shown in **Fig. A-6b**. The errors are smaller than those of the windowing methods already discussed in this Appendix, especially for the Gaussian interpolation.

A.7. Blackman-Harris windowing

The Blackman-Harris window is defined (similarly to (14)) as

$$w_{bmh}(t) = w_r(t)\sum_{i=0}^{3} c_i \cos\left(\frac{2\pi i}{L}t\right) \qquad \text{(A-9)}$$

where $c_0 = 0.40217$, $c_1 = 0.49703$, $c_2 = 0.09892$, $c_3 = 0.00188$.

The corresponding magnitude spectrum, plotted in **Fig. A-7**, is described as for the four-term cosine window in (15). Note that changing these coefficients to those of the BHN window substantially reduces the first sidelobe. See **Table 1** for details.

The errors of the parabolic and Gaussian interpolation with Blackman-Harris windowing, calculated according to (18) and (22) respectively, are shown in **Fig. A-7b**. The errors are considerably bigger than those of BHN windowing, especially for the Gaussian interpolation.

A.8. Nuttall windowing

The Nuttall window is defined as in (A-9) with coefficients $c_0 = 0.3635819$, $c_1 = 0.4891775$, $c_2 = 0.1365995$ and $c_3 = 0.0106411$.

The corresponding magnitude spectrum is presented in **Fig. A-8a**. It is described as for the four-term cosine window in (15). The highest sidelobe is even 5 dB lower than that of BHN windowing. On the other hand, the sidelobe asymptotic fall-off is only 6 dB per octave, while for the BHN window it is three times faster. For that reason the BHN window is considered as the best and was used for interpolation examples presented earlier.

The errors of the parabolic and Gaussian interpolation with Nuttall windowing, calculated according to (18) and (22) respectively, are shown in **Fig. A-8b**. The errors are very similar to those obtained with BHN windowing.